ACS APPLIED MATERIALS & INTERFACES

Research Article

www.acsami.org

KCN Chemical Etch for Interface Engineering in $Cu_2ZnSnSe_4$ Solar Cells

Marie Buffière,*[,†,‡,△] Guy Brammertz,[‖,⊥] Sylvester Sahayaraj,[‡,‖,⊥] Maria Batuk,[#] Samira Khelifi,[□] Denis Mangin,[○] Abdel-Aziz El Mel,[§] Ludovic Arzel,[§] Joke Hadermann,[#] Marc Meuris,[‖,⊥] and Jef Poortmans[†,‡,‖]

[†]imec−partner in Solliance, Kapeldreef 75, 3001 Leuven, Belgium

[‡]Department of Electrical Engineering (ESAT), KU Leuven, Kasteelpark Arenberg 10, 3001 Heverlee, Belgium

[§]Institut des Matériaux Jean Rouxel, Université de Nantes, CNRS, 2 rue de la Houssinière B.P. 32229, 44322 Nantes cedex 3, France

[‖]imec division IMOMEC−partner in Solliance, Wetenschapspark 1, 3590 Diepenbeek, Belgium

[⊥]Institute for Material Research (IMO), Hasselt University, Wetenschapspark 1, 3590 Diepenbeek, Belgium

[#]Electron Microscopy for Materials Science (EMAT), University of Antwerp, Groenenborgerlaan 171, 2020 Antwerp, Belgium

[□]Electronics and Information Systems department (ELIS), University of Gent, Sint-Pietersnieuwstraat 41, 9000 Gent, Belgium

[○]Institut Jean Lamour, Université de Lorraine, Parc de Saurupt, CS 50840, 54011 Nancy, France

[△]Qatar Environment and Energy Research Institute (QEERI), Qatar Foundation, Doha, Qatar

Supporting Information

ABSTRACT: The removal of secondary phases from the surface of the kesterite crystals is one of the major challenges to improve the performances of $Cu_2ZnSn(S,Se)_4$ (CZTSSe) thin film solar cells. In this contribution, the KCN/KOH chemical etching approach, originally developed for the removal of Cu_xSe phases in $Cu(In,Ga)(S,Se)_2$ thin films, is applied to CZTSe absorbers exhibiting various chemical compositions. Two distinct electrical behaviors were observed on CZTSe/CdS solar cells after treatment: (i) the improvement of the fill factor (FF) after 30 s of etching for the CZTSe absorbers showing initially a distortion of the electrical characteristic; (ii) the progressive degradation of the FF after long treatment time for all Cu-poor CZTSe solar cell samples. The first effect can be attributed to the action of KCN on the absorber, that is found to clean the absorber free surface from most of the secondary phases surrounding the kesterite grains (e.g., Se^0, Cu_xSe, $SnSe_x$, SnO_2, Cu_2SnSe_3 phases, excepting the ZnSe-based phases). The second observation was identified as a consequence of the preferential etching of Se, Sn, and Zn from the CZTSe surface by the KOH solution, combined with the modification of the alkali content of the absorber. The formation of a Cu-rich shell at the absorber/buffer layer interface, leading to the increase of the recombination rate at the interface, and the increase in the doping of the absorber layer after etching are found to be at the origin of the deterioration of the FF of the solar cells.

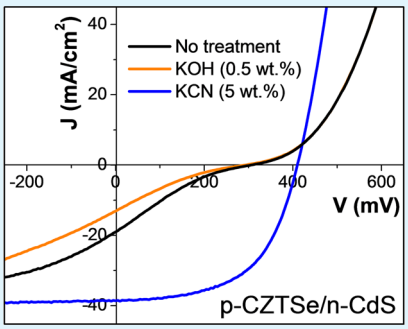

KEYWORDS: *kesterite, CZTSe, KCN, surface, selective etching, photovoltaic*

INTRODUCTION

Considered as a promising technology for substituting $Cu(In,Ga)(S,Se)_2$ (CIGSSe) and CdTe photovoltaic devices because of its low-toxicity and earth-abundant constituent elements, $Cu_2ZnSn(S,Se)_4$ (CZTSSe) thin film solar cells have attracted increasing attention during the past decade, achieving recently a record efficiency of 12.7%.[1−3] CZTSSe compounds are p-type semiconductors, with high absorption coefficients ($>1 \times 10^4$ cm^{-1}) and a direct band gap that can be easily tuned from 1 to 1.5 eV depending on the [S]/([S]+[Se]) ratio.[4−6] Thanks to these unique properties, CZTSSe technology was considered as a promising candidate for a wide range of applications.[7−9] However, the limited control of the composition and the microstructure observed so far in such materials because of the limited stability of the kesterite compound[10] could be considered as a bottleneck for its industrial implementation. Various secondary phases, such as Zn(S,Se), $Cu_x(S,Se)$, $Sn(S,Se)_x$ or $Cu_2Sn(S,Se)_3$, can be formed during the processing of the absorber layer and eventually hinder the electrical performances of the devices.[11−14] This is particularly the case when the CZTSSe layers are prepared under Sn-rich ([Zn]/[Sn]< 1) and Cu-rich ([Cu]/(Sn]+[Zn])> 1) conditions, which enhance the formation of low band gap Sn(S,Se) or $Cu_2Sn(S,Se)_3$ and p-type degenerated $Cu_x(S,Se)$ secondary

Received: March 11, 2015
Accepted: June 3, 2015
Published: June 3, 2015

DOI: 10.1021/acsami.5b02122
ACS Appl. Mater. Interfaces 2015, 7, 14690−14698

phases. As a consequence, the best CZTSSe solar cells (i.e., efficiency >5%) have been prepared under Cu-poor ([Cu]/([Sn]+[Zn]) ~ [0.7;0.95]) and Zn-rich ([Zn]/[Sn] ~ [1.0;1.25]) conditions;[1−3,15−17] in such case, the Zn excess is found to form Zn-rich secondary phases mainly located at the grain boundaries and at the free surface of the CZTSSe grains.[18,19] In most cases, however, the CZTSSe layer is found to also contain some residue of the other secondary phases, even if their formation was prevented by using optimal precursor compositions and synthesis conditions.[18]

Applying a chemical wet etching step is the classical route to selectively remove the secondary phases that could be present on the surface of CZTSSe thin films (i.e., at the p/n junction in the CZTSSe−CdS−ZnO solar cell structure). Different specific procedures were previously developed to etch each of the identified secondary phases. Although the immersion of the CZTSSe samples in hot HCl solution (10 wt %) is adapted to remove ZnS compounds at the surface of the absorber layer,[20] $(NH_4)_2S$ treatment (22 wt %) is found to efficiently etch Sn(S,Se) clusters formed because of a stoichiometric deviation or by condensation.[21] Br_2/MeOH (1 wt %) was reported to remove Cu−Sn−Se-related secondary phases.[22] However, the most common etching approach used so far in literature is based on KCN solution.[22−25] The KCN treatment has been originally developed for CIGSSe thin films and is used for the selective removal of Cu-rich phases such as $Cu_x(S,Se)$ that are known to induce shunting issues in the devices.[26] Concerning CZTSSe compounds, the standard KCN etching process consists in dipping the as-synthesized CZTSSe layer for 2 min in a 5−10 wt % KCN aqueous solution containing KOH for safety reasons.[27] Timmo et al. have shown that such KCN treatment applied to CZTSSe monograins mainly dissolves Cu, Sn and chalcogens.[28] Photoemission studies reported by Bär et al. confirmed that KCN preferentially etches Cu and, to a lesser degree, Sn from CZTS surface, leading to an increase in the surface band gap.[29] In a previous work, we have shown that using a KCN etching step can help recovering a decent minority carrier lifetime for air-exposed CZTSe samples.[30] However, the necessity of such chemical treatment to prepare high efficiency kesterite solar cells is still open to discussion. To provide more elements to answer this question, here we report on the impact of the nominal composition of the absorber and of the KCN etching duration on the properties of CZTSe solar cells. A detailed analysis, consisting of chemical, physical, and electrical measurements, was carried out on the devices.

RESULTS AND DISCUSSION

Impact of the Standard Wet KCN Treatment on CZTSe Thin Films. The chemical composition and the microstructure of different CZTSe layers before and after a standard KCN treatment (i.e., carried out for 120 s at 20 °C using a 5 wt % KCN aqueous solution in 0.5 wt % KOH) were first studied. For this purpose, four CZTSe thin films were synthesized using different Cu precursor layer thicknesses (101 nm (sample code: Cu101), 117 nm (sample code: Cu117), 133 nm (sample code: Cu133), and 149 nm (sample code: Cu149)), whereas the thicknesses of the CuSn and Zn layers were kept constant (see the Supporting Information, section I.A). Figure 1a−h shows top view secondary electron microscopy (SEM) images of these CZTSe samples before (left column) and after KCN treatment (right column). The EDS analysis of the samples is presented in Figure 1i. As expected, increasing the Cu content in the precursor films results in a linear increase in the [Cu]/([Zn]+[Sn]) ratio of the CZTSe films, from 0.62 to 0.98. It also leads to the modification of the [Zn]/[Sn] ratio (that varies between 0.94 and 1.19), as the initial Cu content may influence the formation of volatile secondary phases such as SnSe and Zn. As a consequence, different CZTSe surface morphologies were obtained. Concerning the as-grown samples, some features are visible on the surface of the CZTSe thin films, such as droplets of secondary phases with a size ranging between a few and hundreds of nanometers (Figure 1a, b) as well as nanoneedles of elemental Se (Figure 1d) that can originate from either the stoichiometric deviation during the growth or the condensation of the gaz phases. In case of sample Cu133, the light gray areas visible on Figure 1c

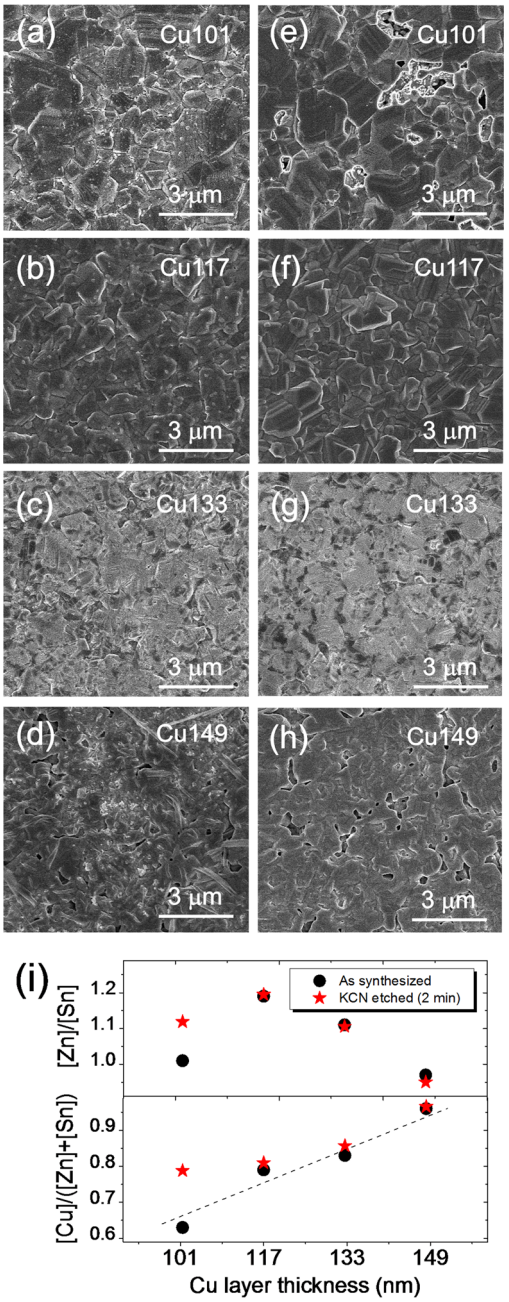

Figure 1. Top-view SEM images of CZTSe layers with different initial Cu contents (a−d) before and (e−h) after dipping in KCN solution for 120 s. The evolution of the [Zn]/[Sn] and the [Cu]/([Zn]+[Sn]) ratios of the samples as found by EDS at 20 kV is plotted in panel i.

DOI: 10.1021/acsami.5b02122
ACS Appl. Mater. Interfaces 2015, 7, 14690−14698

are due to the presence of ZnSe at the surface of the material.[31] After KCN etching, most of these in-homogeneities were removed, except in case of sample Cu133. In the case of the most Cu-poor CZTSe sample (Cu101), large holes were observed (Figure 1e) that may originate from the removal of large crystals of secondary phases. This assumption is supported by the change in the overall composition of the Cu101 CZTSe layer after etching (i.e., the film is less rich in Sn), whereas the [Cu]/([Zn]+[Sn]) and [Zn]/[Sn] ratios remain quasi-constant for the other samples. Raman spectroscopy and X-ray diffraction analysis performed on these samples also confirmed that the Cu101 thin film has its overall structure modified after exposure to KCN due to the removal of secondary phases, such as Cu_2SnSe_3, Sn_xSe, and Cu_xSe (see the Supporting Information, section II.A).

Inductively coupled plasma atomic emission spectroscopy (ICP-AES) analysis was performed on the KCN solutions after different etching durations (30, 60, 200, and 600 s) applied to the Cu117 sample (Figure 2a). The ICP-AES measurements

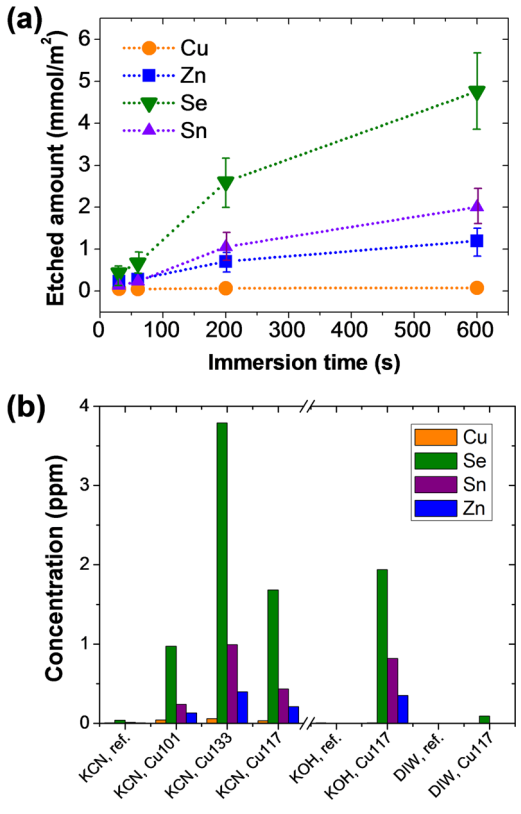

Figure 2. (a) Evolution of the chemical concentrations of Cu, Zn, Sn, and Se as found by ICP-AES measurements performed on the KCN solution samples after different immersion times of Cu117 CZTSe sample; (b) comparison between the chemical concentrations of Cu, Zn, Sn, and Se in the etchant solutions after 120 s of immersion time of the Cu101, Cu117, and Cu133 CZTSe samples in KCN/KOH, KOH, or DIW.

revealed the removal of Se, Sn and, in less extend, Zn from the absorber layer. The proportion in Se:Sn:Zn remains relatively constant (atomic ratio close to 3:1:1) for the different immersion durations. Furthermore, the etching rates of these elements are quasi-linear (taking into account the error bars). As the etched amount after 600 s could not be explained only by the etching of the secondary phases (according to the XRD diagram of the Cu117 sample, see Supporting Information), one can conclude that these Se, Sn and Zn atoms present in the solutions are the products of a preferential etching of the CZTSe phase. It is important to mention that a negligible amount of Cu was detected in the solutions. This appears to be in contradiction with the previous reports on the impact of KCN on CZTS thin films[29] and CZTSSe monograins;[28] this might be related to the different nature of the kesterite samples considered in our study compared to literature (i.e., relatively low amount of Cu_xSe phase). The etched amounts suggest that the free surfaces of the CZTSe crystals should become more Cu-rich after a long KCN etching. Figure 2b shows that the preferential etching of Se, Sn, and Zn from the CZTSe free surfaces can be confirmed for other CZTSe samples (Cu101 and Cu133). To better understand the underlying mechanisms of this preferential etching process, we also performed ICP-AES measurements on KOH solution (0.5 wt %) and pure deionized water (DIW) samples in which the Cu117 sample was immersed for 120 s. As similar etched amounts of Se, Sn, and Zn were found in the KCN/KOH and KOH solutions (whereas only 0.2 ppm of Se was measured in the DIW sample), it can be concluded that the preferential etching of these elements during the KCN treatment is a consequence to the presence of KOH in the solution. This could be due to the presence of stable hydroxide-based complex ions with Sn and Zn, which can be easily formed because of their relatively high oxidation states in CZTSe (+IV and +II for Sn and Zn, respectively) compared to Cu (+I).

To assess the effect of the KCN/KOH etching on the chemical surface structure in detail, we performed X-ray photoelectron spectroscopy (XPS) analyses on the samples (Cu101, Cu117, Cu133, and Cu149) before and after a KCN treatment of 120 s (Figure 3a–l). The high-resolution scans of the Sn $3d_{5/2}$ XPS lines show that, for all the samples, the FWHM of the signal decreases after etching in KCN because of the vanishing of a high binding energy (BE) contribution to the signal (as clearly observed for the sample Cu149, where this contribution leads to the formation of a shoulder at 487.5 eV). Most probably, this contribution may originate from Sn-based secondary phases that were etched from the absorber surface upon exposure to KCN, in agreement with the SEM images of the cleaned surfaces obtained after treatment (Figure 1). In the meantime, the O 1s and Se 3d spectra also shows multiple contributions to the XPS signals (except in the case of the sample Cu 117). For the O 1s signal, the two contributions located at 530.3 and 531.6 eV are simultaneously reduced after treatment. For the Se 3d spectra, the additional contributions seem to be reduced while the one coming from the CZTSe/ZnSe material is enhanced. Therefore, this Sn-based secondary phases can be SnO_2 or/and $SnSe_2$ compounds, since it contains Sn with an oxidation state similar to the one present in the CZTSe phase (i.e., very close BE values) and that no additional Cu or Zn contribution can be extracted from the XPS signals. In case of the Cu101, Cu133, and Cu149 samples, as the intensity of the O 1s signal decreases while the one of Se 3d peaks increases after KCN, the decrease in the FWHM of the Sn 3d XPS peaks can be explained by the partial removal of SnO_2. For the sample Cu117, the Sn $3d_{5/2}$ signal can also be fitted with two contributions; however, in this particular case, it is the intensity of the low BE contribution at 486.3 eV attributed to the CZTSe phase that slightly decreases after treatment. This might be due to the preferential etching of Sn detected by ICP-AES, that become more visible as this sample

DOI: 10.1021/acsami.5b02122
ACS Appl. Mater. Interfaces 2015, 7, 14690–14698

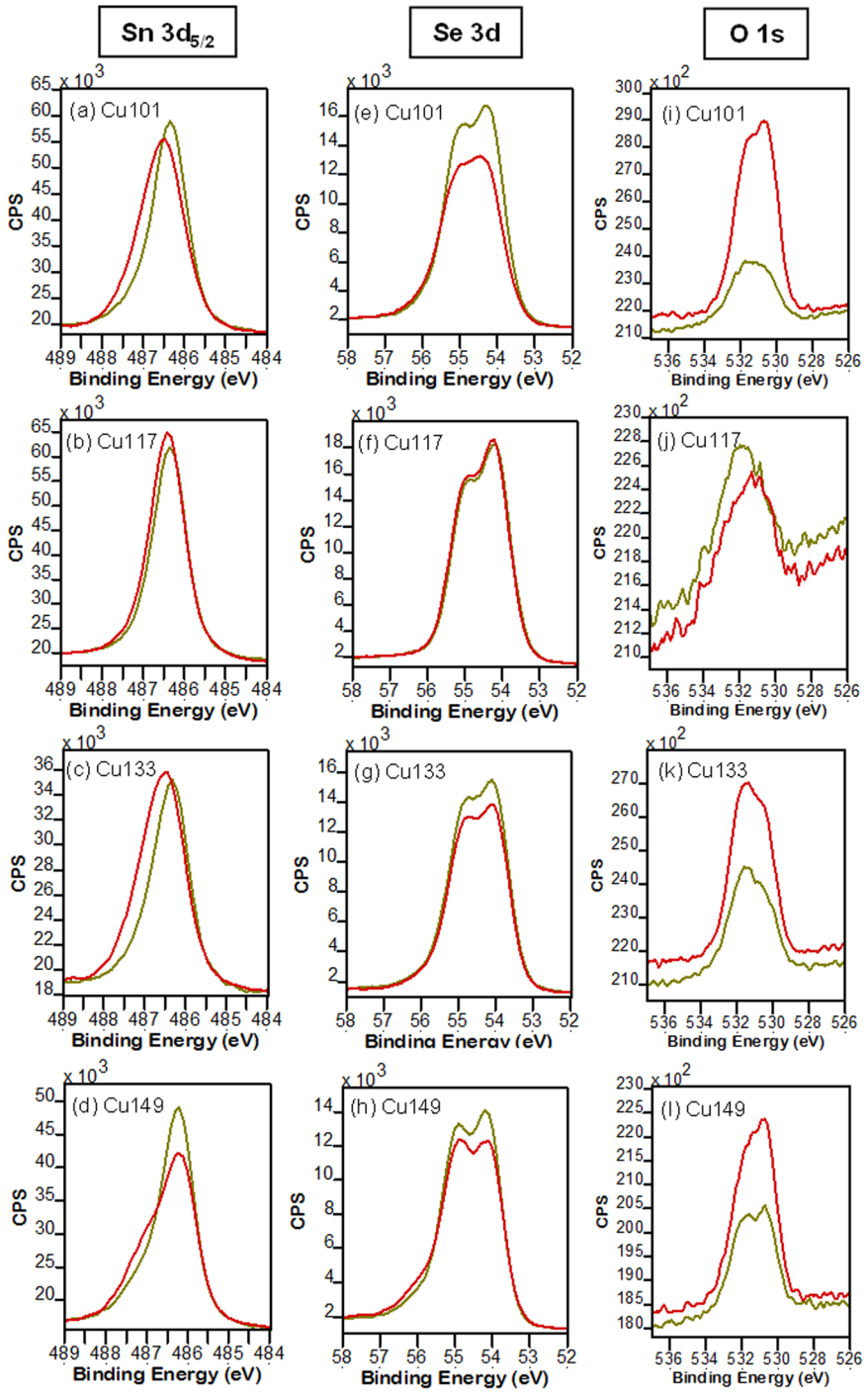

Figure 3. Sn $3d_{5/2}$, Se 3d, and O 1s XPS peaks recorded on Cu101, Cu117, Cu133, and Cu149 before (red) and after (green) treatment in KCN for 120 s.

contains few secondary phases (according to the low oxygen content and the Se 3d signals that can be fitted with only one contribution for each peak). The comparative analysis of the samples before and after KCN treatment also reveals that, in our case, the Cu content at the surface of the absorber slightly increases after the KCN treatment, except in the case of the Cu117 for which the Cu content stays rather constant (see Supporting Information, part II.B). This would mean that the preferential etching of Sn, Zn and Se does not necessarily take place at the top surface of the absorber. Indeed, as many voids are usually observed at the back contact/absorbers interfaces and as the etching solution could easily penetrates these voids, the preferential etch might also take place in this region of the absorber. The low amount of Cu measured on all the CZTSe surfaces has been already reported elsewhere[32] and could be compared to the Cu-depletion observed at the surface of CIGSe absorbers.[33] We also observed that the Zn content measured before and after KCN etching is quite similar. The sample Cu133 shows a high Zn and Se concentration with a ratio close to 1; this confirms the presence of a large amount of ZnSe at the surface of such absorber that is not removed after treatment. The KCN etch is also found to remove the Na

DOI: 10.1021/acsami.5b02122
ACS Appl. Mater. Interfaces 2015, 7, 14690−14698

accumulated at the surface of the sample (see the Supporting Information, section II.B).

Influence of the KCN Treatment Duration on CZTSe Solar Cells. In this section, we investigate the impact of the KCN/KOH etch on the electrical performances of CZTSe-CdS-ZnO solar cells prepared with the Cu101, Cu117, Cu133 and Cu149 absorber layers. In Figure 4a–d, the *I*–*V* curves

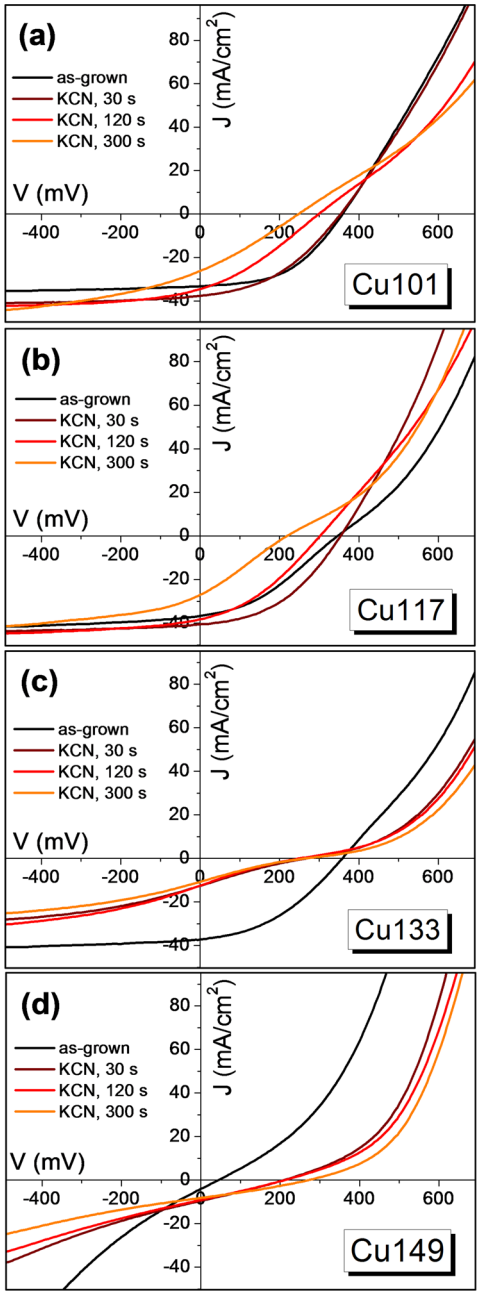

Figure 4. *I*–*V* curves of CZTSe–CdS–ZnO solar cells prepared from (a) Cu101, (b) Cu117, (c) Cu133, and (d) Cu149 treated in KCN for different durations (0, 30, 120, and 300 s).

measured on four series of solar cells are presented; for each series the same CZTSe absorber etched for different durations in KCN (i.e., 0, 30, 120, or 300 s) was used. It can be clearly remarked that the impact of the KCN etch on the solar cell performances depends on the chemical composition of the CZTSe absorber. For the most Cu-poor sample (Figure 4a), the J_{sc} is improved after 30 s of KCN etch, resulting in an improvement of the efficiency of the device. When increasing the treatment duration, a kink appears on the I–V curve leading, at first, to a decrease in the V_{oc} and the FF, and then in the J_{sc} of the device. Considering our previous observation on the effect of KOH and KCN on the chemical composition at the CZTSe surface, we suggest that the improvement of the J_{sc} in the case of the Cu101 sample is due to the removal of the secondary phases, while the KOH would be responsible for the progressive degradation of the FF when increasing the treatment duration, due to the preferential etching of Se, Sn and Zn from the surfaces of the absorber. In the case of the sample Cu117 (Figure 4b), an improvement of the efficiency is also revealed after 30 s of KCN etch, mainly due to the improvement in the FF, as the kink present on the as-grown reference sample disappears after treatment. Here again, increasing the KCN etching duration to 120 s and then to 300 s leads to a distortion in the *I*–*V* curve, which increases with increasing treatment time. In this case, the origin of the improvement of the efficiency after 30 s of treatment is less obvious, as this absorber contains a low amount of secondary phases. However, it cannot be excluded that secondary phases are present around the voids at the back/absorber interfaces forming a barrier to the holes transport, and could be etched by the KCN solution. Complementary electrical results obtained on CZTSe solar cells showing initially a large *I*–*V* distortion and treated in KCN (without KOH) or in KOH (without KCN) tend to confirm that the FF improvement is due to the KCN, whereas KOH degrades the FF (see the Supporting Information, section II.E).

For the series using the Cu133 absorber (Figure 4c), the KCN etch quickly leads to a drastic decrease of all the electrical parameters due to a very strong distortion of the characteristic. This might be due to the particular surface of this sample, which contains a large amount of ZnSe phase. As the KCN/KOH does not affect this phase, the action of the etchant will be focused on the small domains of CZTSe accessible to the solution. Therefore, the preferential etching of Se, Sn, and Zn is concentrated on these areas and severely affect the properties of the p/n junction. Finally, the as-grown reference sample using the most Cu-rich absorber (Cu149, Figure 4d) is found to be shunted, due to the presence of Cu_xSe phases. Therefore, the KCN treatment carried out on this type of absorber slightly improves the efficiency of the devices.

Furthermore, more detailed electrical characterizations were performed on the Cu101 solar cells with different treatment durations. Figure 5a shows the doping profile derived from Mott–Schottky plot of capacitance–voltage (*C*–*V*) measurements. It can be seen that the doping of the CZTSe absorber increases by 1 order of magnitude when increasing the immersion time in the KCN/KOH solution from 0 to 300 s, therefore decreasing the apparent space charge region (SCR) width in the absorber. The external quantum efficiency (EQE) spectra of these solar cells measured without intentional light bias reveal that the maximum EQE value (at 500 nm) increases after 30 s of treatment, and decreases after a longer treatment duration. This evolution of the shape of the EQE can be due to the modification of the SCR width. When using light bias, the collection of the photoelectron is improved on the whole wavelength range (giving J_{sc} values close to the one measured by *I*–*V*), showing the presence of a light sensitive barrier. Finally, *I*–*V* measurements as a function of the temperature (*I*–*V*–*T*) show that the extrapolation of the qV_{oc} value

DOI: 10.1021/acsami.5b02122
ACS Appl. Mater. Interfaces 2015, 7, 14690–14698

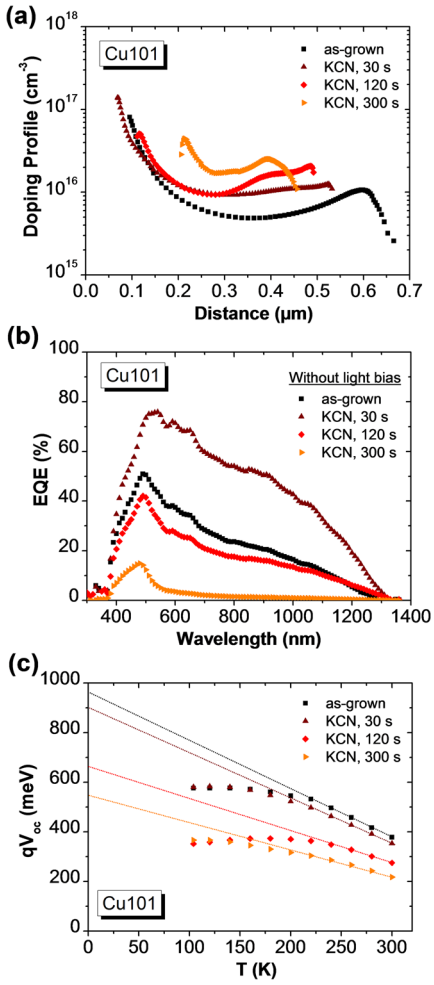

Figure 5. (a) Doping profile derived from Mott–Schottky plot, (b) EQE spectra, and (c) evolution of the V_{oc} as a function of temperature measured on Cu101 solar cells using different durations of KCN etch (0, 30, 120, and 300 s).

progressively decreases as the etching duration increases from 0 to 300 s, meaning that the main location of the limiting recombination mechanisms is moving from bulk to interface.

To determine the physical origins of these electrical phenomena, we analyzed complete devices by scanning transmission electron microscopy (STEM) and secondary ions mass spectroscopy (SIMS). At first, STEM-EDS mapping was carried out on the Cu101 solar cells synthesized with and without a standard KCN treatment. Figure 6a, c show HAADF-STEM images of both samples. In both cases, the thickness of the CZTSe layers varies from 900 nm to ∼1.15 μm and consists of large (∼800 nm) densely packed grains of an irregular shape. Large holes were observed at the CZTSe/Mo interface, as already reported.[18] However, the grain boundaries of the nontreated sample are more visible, meaning that they likely contain more chemical and structural nonhomogeneity. According to the EDS maps acquired on this sample (Figure 6c), this specimen contains a lot of inclusions of secondary phases, mainly located at the grain boundaries and close to the interfaces. Within the CZTSe layer, we found some inclusions of ZnSe randomly distributed within the CZTSe layer (as indicated with the blue arrows on Figure 6). The Zn:Se atomic ratio in these areas is very close to 1:1. There are also large inclusions of the ternary Cu_xSnSe_y phases (indicated with pink

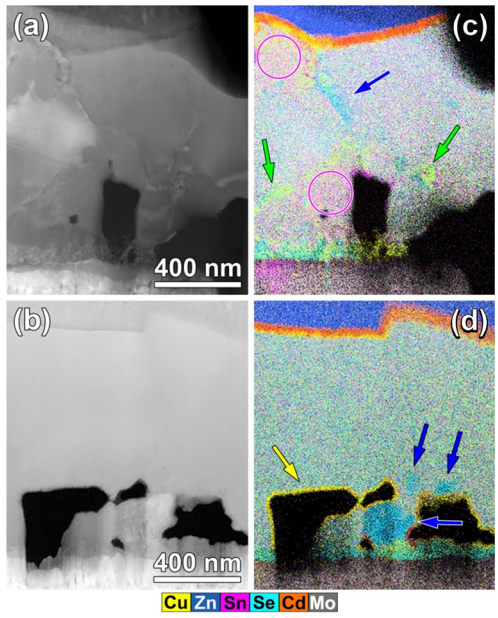

Figure 6. HAADF-STEM images and the corresponding overlaid RGB images of the Cu–K, Zn–K, Sn-L, Se–K, Cd–L, and Mo–K EDS dynamic maps recorded on a Cu101 solar cell prepared (a, c) without and (b, d) with a KCN treatment for 120 s.

circles). An average Cu:Sn:Se ratio measured from four areas is 32:16:52. Some tiny Cu_xSe clusters were also observed (as pointed out on Figure 6c with green arrows). No $SnSe_x$ phases could be detected on this specimen at the surface region of the sample; this may appear in contradiction with our XPS results, but could be due to the very small area measured by STEM compared to XPS. The CZTSe/Mo interface shows not only inclusions of ZnSe and Cu_xSnSe_y, but also Cu_xSe and Zn_xSnSe_y (see the Supporting Information, section II.C). We also observed that the CdS layer on top of the CZTSe layer is not completely uniform, with some area contaminated with Cu (likely originating from the Cu_xSe phase). The Cu101 CZTSe absorber seems more homogeneous after KCN treatment (Figure 6d), as only ZnSe inclusions located at the back interface could be observed. However, a layer as thin as ∼20 nm was found to surround the free surface of the bottom CZTSe grains (indicated with a yellow arrow). The EDS maps recorded on this area show that this layer mainly contains Cu, Cd, and S, in different proportions depending on the analyzed area (see t he Supporting Information, section II.C). This layer could have been formed first during the KCN etch, then during the deposition of the n-type CdS buffer layer, through the pinholes in the CZTSe film observed after KCN etching (Figure 1e). Also, a continuous Cu-rich layer is formed at the CZTSe/CdS interface; this is in good agreement with the previous ICP-AES and XPS results, showing that this Cu-rich layer is formed during the chemical treatment. Therefore, despite the quality improvement of the kesterite absorber, the degradation of the CZTSe/CdS interface due to the Cu-rich interlayer and/or the presence of a thin Cu:Cd:S layer at the free surface of the CZTSe grains could be responsible for the distortion of the electrical characteristics of the CZTSe solar cells revealed after treatment. When increasing the etching time, this effect becomes more visible as a thicker Cu-rich interlayer/capping layer can be formed. This supposition is in good agreement with most of literature reporting on CZTSe

DOI: 10.1021/acsami.5b02122
ACS Appl. Mater. Interfaces 2015, 7, 14690–14698

and CIGSe solar cells, which show that the distortion of I−V curves in thin film solar cells can be explained by interface issues (e.g., presence of a potential barrier in the region of the heterojunction).[34,35] This barrier may be responsible for the increase in the photocarrier recombination rate observed at the interface when increasing the treatment duration. Furthermore, it is well-known that the CdS compound itself is a photosensitive material, for which the doping depends on the illumination conditions.[36] By extrapolation, the mixed Cu:Cd:S compound could also be photosensitive; this would explain the difference in the EQE spectra measured with and without light bias.

Additionally, SIMS measurements were performed on the 4 samples using the Cu117 absorber. The concentrations in alkali atoms (Na, K), which originally diffuse from the glass substrate

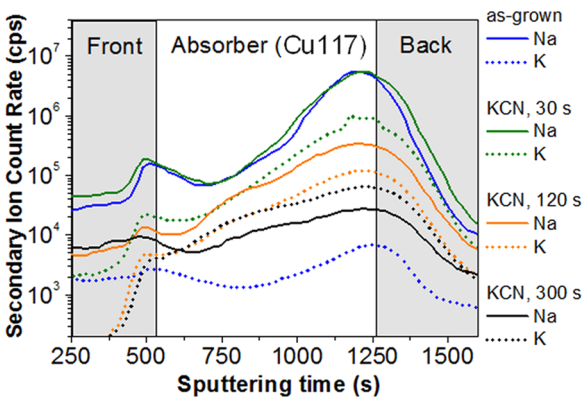

Figure 7. ^{23}Na and ^{39}K SIMS depth profiles recorded through Cu117 solar cells synthesized without and with 30 s, 120 s, 300 s of KCN etch.

during the annealing stage, were followed. Figure 7 shows the ^{23}Na and ^{39}K SIMS depth profiles through the Cu117 solar cells synthesized without and with 30 s, 120 or 300 s of KCN etch. All the alkali profiles measured on the samples exhibit a V-shape profile. Indeed, as our kesterite absorbers can be considered as porous structures due to the large amount of holes at the back side of the absorbers, the surface-to-bulk ratio of the CZTSe thin films is relatively high and the apparent "bulk" of the absorber contains some voids. In CZTSe polycrystalline thin films, Na (and likely K) atoms are mainly located at the free surface and grain boundaries.[38] As the KCN solution could easily interpenetrate the porous CZTSe structure and modify the alkali content on the free surfaces (and eventually at the grain boundaries) of the absorber, the Na/K concentrations is found to be proportional to the surface/bulk ratio as a function of the analysis depth. After 30 s of treatment, the Na concentration in the CZTSe layer appears to remain similar to the one measured without etching. As the KCN etch duration increases from 30 to 300 s, the Na content in the absorber decreases by 2 orders of magnitude. It can be also remarked that the K content increases after KCN treatment; the extra-potassium atoms measured in the absorber may originate either from KCN or KOH present in the etching solution. The modification of both Na and K contents in the absorber as a function of the treatment time could eventually contribute to a change of doping in the absorber.[37] This change of doping could also be at the origin of the vanishing of the initial kink after 30 s of treatment observed for this sample. Also, according to the SIMS profiles, it seems that both Na and K concentrations mainly change at the back side of the absorber after KCN treatment, where the S content was found to slightly increase (see the Supporting Information, section II.D) because of the formation of the Cu:Cd:S layer. Therefore, the appearance of the kink could be also due to the modification of the alkali content at the free CZTSe surface close to the Mo back contact and/or at the CZTSe/CdS interface.

CONCLUSION

In summary, the effect of the standard wet KCN/KOH treatment on the properties of the interfaces in CZTSe solar cells was investigated. From the physical characterization of the samples, the KCN treatment is found to selectively etch most of the secondary phases that can be formed at the free surface of the CZTSe thin films (i.e., Se^0, Cu_xSe, Cu_xSnSe_y, $SnSe_2$ and SnO_2) except ZnSe, whereas the KOH present in the KCN solution, added in general for safety reasons, preferentially reacts with the Se, Sn, and Zn of the CZTSe phase leading to an increase in the Cu content at the surface of the CZTSe absorber. The etching solution was also found to modify the alkali content (Na, K) content of the absorber, whereas the bulk concentrations in Cu, Zn, Sn, and Se remain constant (except in case of large amount of secondary phases). As a consequence, two distinct phenomena were observed on the electrical characteristic of the CZTSe solar cells: (i) the improvement of the efficiency after only 30 s of treatment, for the devices showing initially a distortion of the *I*−*V* curve; (ii) the progressive decrease in the FF of the solar cells when increasing the treatment duration. This later observation is a consequence of the increase of the doping of the absorber combined with the presence of a barrier at the p/n junction that increase the recombination rate at this interface, likely due to the degradation of the free surface of the CZTSe grains that become more Cu-rich. Therefore, it is recommended to limit the duration of the KCN treatment to 30 s and/or to reduce the concentration of KOH in solution for the processing of high-efficiency CZTSe solar cells.

ASSOCIATED CONTENT

Supporting Information

Experimental methods, characterization techniques, and further physical and electrical characterization of the devices. The Supporting Information is available free of charge on the ACS Publications website at DOI: 10.1021/acsami.5b02122.

AUTHOR INFORMATION

Corresponding Author

*E-mail: marie.buffiere@outlook.com.

Author Contributions

The manuscript was written through contributions of all authors. All authors have given approval to the final version of the manuscript.

Notes

The authors declare no competing financial interest.

ACKNOWLEDGMENTS

This research is partially funded by the Flemish government, Department Economy, Science and Innovation. We acknowledge Flamac at Gent for the sputter-deposition of the metal layers. AGC is acknowledged for providing SLG/Mo substrates

DOI: 10.1021/acsami.5b02122
ACS Appl. Mater. Interfaces 2015, 7, 14690−14698

REFERENCES

(1) Kim, J.; Hiroi, H.; Todorov, T. K.; Gunawan, O.; Kuwahara, M.; Gokmen, T.; Nair, D.; Hopstaken, M.; Shin, B.; Lee, Y. S.; Wang, W.; Sugimoto, H.; Mitzi, D. B. High Efficiency $Cu_2ZnSn(S,Se)_4$ Solar Cells by Applying a Double In_2S_3/CdS Emitter. *Adv. Mater.* **2014**, *26*, 7427−7431.

(2) Repins, I.; Beall, C.; Vora, N.; DeHart, C.; Kuciauskas, D.; Dippo, P.; To, B.; Mann, J.; Hsu, W.-C.; Goodrich, A.; Noufi, R. Co-evaporated $Cu_2ZnSnSe_4$ Films and Devices. *Sol. Energy Mater. Sol. Cells* **2012**, *101*, 154−159.

(3) Brammertz, G.; Ren, Y.; Buffière, M.; Mertens, S.; Hendrickx, S.; Zaghi, A. E.; Lenaers, N.; Köble, C.; Meuris, M.; Poortmans, J. Correlation between Physical, Electrical, and Optical Properties of $Cu_2ZnSnSe_4$ Solar Cells. *Thin Solid Films* **2013**, *535*, 348−352.

(4) Siebentritt, S.; Schorr, S. Kesterites—a Challenging Material for Solar Cells. *Prog. Photovolt: Res. Appl.* **2012**, *20*, 512−519.

(5) Delbos, S. Këesterite Thin Films for Photovoltaics: a Review. *EPJ. Photovoltaics* **2012**, *3*, 35004.

(6) Persson, C. Electronic and Optical Properties of Cu_2ZnSnS_4 and $Cu_2ZnSnSe_4$. *J. Appl. Phys.* **2010**, *107*, 53710.

(7) He, J.; Lee, L.; Yang, S.; Li, Q.; Xiao, X.; Chen, T. Printable Highly Catalytic Pt- and TCO-Free Counter Electrode for Dye-Sensitized Solar Cells. *ACS Appl. Mater. Interfaces* **2014**, *6*, 2224−2229.

(8) Ma, G.; Minegishi, T.; Yokoyama, D.; Kubota, J.; Domen, K. Photoelectrochemical Hydrogen Production on Cu_2ZnSnS_4/Mo-mesh Thin-Film Electrodes Prepared by Electroplating. *Chem. Phys. Lett.* **2011**, *501*, 619−622.

(9) Wang, G.; Zhao, W.; Cui, Y.; Tian, Q.; Gao, S.; Huang, L.; Pan, D. Fabrication of a $Cu_2ZnSn(S, Se)_4$ Photovoltaic Device by a Low-Toxicity Ethanol Solution Process. *ACS Appl. Mater. Interfaces* **2013**, *5*, 10042−10047.

(10) Redinger, A.; Berg, D. M.; Dale, P. J.; Siebentritt, S. The Consequences of Kesterite Equilibria for Efficient Solar Cells. *J. Am. Chem. Soc.* **2011**, *133*, 3320−3323.

(11) Tanaka, T.; Sueishi, T.; Saito, K.; Guo, Q.; Nishio, M.; Yu, K.; Walukiewicz, V. Existence and Removal of Cu_2Se Second Phase in Coevaporated $Cu_2ZnSnSe_4$ Thin Films. *J. Appl. Phys.* **2012**, *111*, 053522.

(12) Just, J.; Lutzenkirchen-Hecht, D.; Frahm, R.; Schorr, S.; Unold, T. Determination of Secondary Phases in Kesterite Cu_2ZnSnS_4 Thin Films by X-ray Absorption Near Edge Structure Analysis. *Appl. Phys. Lett.* **2011**, *99*, 262105.

(13) Redinger, A.; Hönes, K.; Fontané, X.; Izquierdo-Roca, V.; Saucedo, E.; Valle, N.; Pérez-Rodríguez, A.; Siebentritt, S. Detection of a ZnSe Secondary Phase in Coevaporated $Cu_2ZnSnSe_4$ Thin Films. *Appl. Phys. Lett.* **2011**, *98*, 101907.

(14) Brammertz, G.; Oueslati, S.; Buffière, M.; Bekaert, J.; El Anzeery, H.; Messaoud, K. B.; Sahayaraj, S.; Nuytten, T.; Koble, C.; Meuris, M.; Poortmans, J. Investigation of Properties Limiting Efficiency in $Cu_2ZnSnSe_4$ based Solar Cells. *IEEE J. Photovoltaics* **2015**, *5*, 649−655.

(15) Wang, W.; Winkler, M.; Gunawan, O.; Gokmen, T.; Todorov, T.; Zhu, Y.; Mitzi, D. Device Characteristics of CZTSSe Thin-Film Solar Cells with 12.6% Efficiency. *Adv. Energy Mater.* **2014**, *4*, 1301465.

(16) Chawla, V.; Clemens, B. Effect of Composition on High Efficiency CZTSSe Devices Fabricated Using Co-Sputtering of Compound Targets. In *Proceedings of 38th IEEE PVSC Conference*; Austin, TX, June 3−8, 2012 ; IEEE: Piscataway, NJ, 2012.

(17) Scragg, J. J.; Kubart, T.; Wätjen, J. T.; Ericson, T.; Linnarsson, M. K.; Platzer-Björkman, C. Effects of Back Contact Instability on Cu_2ZnSnS_4 Device and Processes. *Chem. Mater.* **2013**, *25*, 3162−3171.

(18) Buffière, M.; Brammertz, G.; Batuk, M.; Verbist, C.; Mangin, D.; Koble, C.; Hadermann, J.; Meuris, M.; Poortmans, J. Microstructural Analysis of 9.7% Efficient $Cu_2ZnSnSe_4$ Thin Film Solar Cells. *Appl. Phys. Lett.* **2014**, *105*, 183903.

(19) Mendis, B.; Goodman, M.; Major, J.; Taylor, A.; Durose, K.; Halliday, D. The Role of Secondary Phase Precipitation on Grain Boundary Electrical Activity in Cu_2ZnSnS_4 (CZTS) Photovoltaic Absorber Layer Material. *J. Appl. Phys.* **2012**, *112*, 124508.

(20) Fairbrother, A.; García-Hemme, E.; Izquierdo-Roca, V.; Fontané, X.; Pulgarín-Agudelo, F. A.; Vigil-Galán, O.; Pérez-Rodríguez, A.; Saucedo, E. Development of a Selective Chemical Etch to Improve the Conversion Efficiency of Zn-rich Cu_2ZnSnS_4 Solar Cells. *J. Am. Chem. Soc.* **2012**, *134*, 8018−8021.

(21) Xie, H.; Sánchez, Y.; López-Marino, S.; Espíndola-Rodríguez, M.; Neuschitzer, M.; Sylla, D.; Fairbrother, A.; Izquierdo-Roca, V.; Pérez-Rodríguez, A.; Saucedo, E. Impact of Sn(S,Se) Secondary Phases in $Cu_2ZnSn(S,Se)_4$ Solar Cells: a Chemical Route for Their Selective Removal and Absorber Surface Passivation. *ACS Appl. Mater. Interfaces* **2014**, *6*, 12744−12751.

(22) Mousel, M.; Redinger, A.; Djemour, R.; Arasimowicz, M.; Valle, N.; Dale, P.; Siebentritt, S. HCl and Br_2-MeOH Etching of $Cu_2ZnSnSe_4$ Polycrystalline Absorber. *Thin Solid Films* **2013**, *535*, 83−87.

(23) Schubert, B.; Marsen, B.; Cinque, S.; Unold, T.; Klenk, R.; Schorr, S.; Schock, H. W. Cu_2ZnSnS_4 Thin Film Solar Cells by Fast Coevaporation. *Prog. Photovolt: Res. Appl.* **2011**, *19*, 93−96.

(24) Oueslati, S.; Brammertz, G.; Buffière, M.; ElAnzeery, H.; Touayar, O.; Köble, C.; Bekaert, J.; Meuris, M.; Poortmans, J. Physical and Electrical Characterization of High-Performance $Cu_2ZnSnSe_4$ based Thin Film Solar Cells. *Thin Solid Films* **2015**, *582*, 224−228.

(25) Jeon, J. O.; Lee, K. D.; Oh, L. S.; Seo, S. W.; Lee, D. K.; Kim, H.; Jeong, J. H.; Ko, M. J.; Kim, B.; Son, H. J.; Kim, J. Y. Highly Efficient Copper-Zinc-Tin-Selenide (CZTSe) Solar Cells by Electrodeposition. *ChemSusChem* **2014**, *4*, 1073−1077.

(26) Buffière, M.; El Mel, A.-A.; Lenaers, N.; Brammertz, G.; Zaghi, A. E.; Meuris, M.; Poortmans, J. Surface Cleaning and Passivation Using $(NH_4)_2S$ Treatment for $Cu(In,Ga)Se_2$ Solar Cells: A Safe Alternative to KCN. *Adv. Energy Mater.* **2015**, *5*, 1401689.

(27) Mousel, M.; Schwarz, T.; Djemour, R.; Weiss, T. P.; Sendler, J.; Malaquias, J. C.; Redinger, A.; Cojocaru-Mirédin, O.; Choi, P.-P.; Siebentritt, S. Cu-Rich Precursors Improve Kesterite Solar Cells *Adv. Energy Mater.* **2014**, *4*, 1300543.

(28) Timmo, K.; Altosaar, M.; Raudoja, J.; Grossberg, M.; Danilson, M.; Volobujeva, O.; Mellikov, E. Chemical Etching of $Cu_2ZnSn(S,Se)_4$ Monograin Powder In *Proceedings of 35th IEEE PVSC*; Hawaii, June 20−25, 2010 ; IEEE: Piscataway, NJ, 2010.

(29) Bär, M.; Schubert, B.-A.; Marsen, B.; Krause, S.; Pookpanratana, S.; Unold, T.; Weinhardt, L.; Heske, C.; Schock, H.-W. Impact of KCN Etching on the Chemical and Electronic Surface Structure of Cu_2ZnSnS_4 Thin-film Solar Cell Absorbers. *Appl. Phys. Lett.* **2011**, *99*, 152111.

(30) Buffière, M.; Brammertz, G. ; El Mel, A.-A. ; Lenaers, N. ; Yi Ren ; Zaghi, A. E. ; Mols, Y. ; Koeble, C. ; Vleugels, J. ; Meuris, M. ; Poortmans, J. Recombination Stability in Polycrystalline $Cu_2ZnSnSe_4$ Thin Films. In *Proceedings of 39th IEEE PVSC*; Tampa, FL, June 16−21, 2013 ; IEEE: Piscataway, NJ, 2013.

(31) Buffière, M.; ElAnzeery, H.; Oueslati, S.; Ben Messaoud, K.; Brammertz, G.; Meuris, M.; Poortmans, J. Physical Characterization of $Cu_2ZnGeSe_4$ Thin Films from Annealing of Cu−Zn−Ge Precursor Layers. *Thin Solid Films* **2015**, *582*, 171−175.

(32) Bär, M.; Schubert, B.-A.; Marsen, B.; Krause, S.; Pookpanratana, S.; Unold, T.; Weinhardt, L.; Heske, C.; Schock, H.-W. Native Oxidation and Cu-poor Surface Structure of Thin Film Cu_2ZnSnS_4 Solar Cell Absorbers. *Appl. Phys. Lett.* **2011**, *99*, 112103.

(33) Chirilă, A.; Reinhard, P.; Pianezzi, F.; Bloesch, P.; Uhl, A. R.; Fella, C.; Kranz, L.; Keller, D.; Gretener, C.; Hagendorfer, H.; Jaeger, D.; Erni, R.; Nishiwaki, S.; Buecheler, S.; Tiwari, A. N. Potassium-induced Surface Modification of $Cu(In,Ga)Se_2$ Thin Films for High-efficiency Solar Cells. *Nat. Mater.* **2013**, *12*, 1107−1111.

(34) Igalson, M.; Urbaniak, A.; Zabierowski, P.; Maksoud, H.; Abdel; Buffière, M.; Barreau, N.; Spiering, S. Red-blue Effect in CIGS Devices Revisited. *Thin Solid Films* **2013**, *535*, 302−306.

(35) Buffière, M.; Brammertz, G.; Oueslati, S.; ElAnzeery, H.; Bekaert, J.; Ben Messaoud, K.; Köble, C.; Khelifi, S.; Meuris, M.;

DOI: 10.1021/acsami.5b02122
ACS Appl. Mater. Interfaces 2015, 7, 14690−14698

Poortmans, J. Spectral Current-voltage Analysis of Kesterite Solar Cells. *J. Phys. D. Appl. Phys.* **2014**, *47*, 175101.
(36) Pudov, A. O.; Kanevce, A.; Al-Thani, H. A.; Sites, J. R.; Hasoon, F. S. Secondary Barriers in CdS-$CuIn_{1-x}Ga_xSe_2$ Solar Cells. *J. Appl. Phys.* **2005**, *97*, 064901.
(37) Li, J. V.; Kuciauskas, D.; Young, M. R.; Repins, I. L. Effects of Sodium Incorporation in Co-Evaporated $Cu_2ZnSnSe_4$ Thin-Film Solar Cells. *Appl. Phys. Lett.* **2013**, *102*, 163905.
(38) Schwarz, T.; Cojocaru-Mirédin, O.; Choi, P.; Mousel, M.; Redinger, A.; Siebentritt, S.; Raabe, D. Atom Probe study of $Cu_2ZnSnSe_4$ Thin-films prepared by Co-evaporation and Post-deposition Annealing. *Appl. Phys. Lett.* **2013**, *102*, 042101.

DOI: 10.1021/acsami.5b02122
ACS Appl. Mater. Interfaces 2015, 7, 14690−14698